Supporting Information

Enhancing electrocatalytic nitrogen reduction on Ce-WO_3 catalysts through atomically local electric field effect: accelerated electron transfer and enhanced nitrogen activation

Hao Che[a], Xiaoxuan Wang*[a], Jingwen Guo [a], Yibo Wang [a], Qi Luo [a], Minglei Wang [a], Jun Xiang [a], Zheng Zhen,[b] Rongda Zhao* [a], Fufa Wu* [C]

[a] *School of Materials Science and Engineering,*
Liaoning University of Technology
Jinzhou, Liaoning Province, 121001, People's Republic of China
[b] *Center for Analysis and Measurement,*
Harbin Institute of Technology,
Harbin 150001, People's Republic of China
[C] *School of Materials Science and Engineering,*
Liaoning Technical University
Fuxin, Liaoning Province, 123032, People's Republic of China

* Corresponding Authors.
E-mail address: clwangxx@lnut.edu.cn; rongdazhaoln@126.com; ffwu@lnut.edu.cn

Experimental Procedures

Chemicals and Materials

Commercial Tungsten Hexachloride (WCl_6) and Cerium Trichloride ($CeCl_3$) were obtained from Shanghai Chemical Reagent Co. Ltd. Hydrazine hydrate ($N_2H_4 \cdot H_2O$) and ethanol (C_2H_5OH) were procured from Sigma-Aldrich chemical company. Salicylic acid ($C_7H_6O_3$, ≥99.7%), ammonium chloride (NH_4Cl, 99.998%), p-dimethylaminobenzaldehyde (p-$C_9H_{11}NO$, 99%), trisodium sodium citrate dehydrate ($C_6H_5Na_3O_7 \cdot 2H_2O$, 99%), sodium nitroferricyanide dihydrate ($C_5FeN_6Na_2O \cdot 2H_2O$, 99%), and sodium hypochlorite solution (NaClO, available chlorine 6-10%) were obtained from Beijing Chemical Corp. Nafion solution (5 wt%) was purchased from Sigma-Aldrich Chemical Reagent Co., Ltd. All chemicals were used without any further purification. Ultrapure Smart-S15 water (18.2 MΩ) was used in all experiments.

Characterizations

To observe the morphology and microstructure of the samples, field emission scanning electron microscopy (SEM, FEI Quanta 200), transmission electron microscopy (TEM, FEI Tecnai G2 20), and high-resolution TEM (HRTEM, JEM-2100F, 200 kV) were employed. The crystalline structures were analyzed using X-ray diffraction (XRD, Rigaku D/max 2500) equipped with Cu Kα radiation (λ = 0.15405 nm). The surface chemical status and composition were analyzed using X-ray photoelectron spectroscopy (XPS, Thermo Fisher Scientific) with an Al Kα X-ray source and Finder Vista Laser micro-Raman Spectroscopy (Zolix, China) with laser excitation of 532 nm. The Kelvin probe force microscopy (KPFM) was obtained to analyze the surface potential of the materials using atomic force microscopy (AFM, Oxford MFP-3D, UK). For *in situ* Raman tests using an excitation wavelength of 532 nm, the electrochemical operando flow cell (EC-RAIR-H) was provided by Tianjin Gaoss Union technology Co. Ltd. A SOPTOP LMPlan objective (50X) was used for signal collection and the collection time was 30 seconds. Laser power was kept below 1.5 mW to protect the sample from laser damage.

Synthesis of electrocatalysts

0.405 g of WCl_6 was added to a beaker containing 60 mL of ethanol and subjected to ultrasonic dispersion for 10 minutes. Subsequently, 0.015 (0.01 and 0.02) g of $CeCl_3$ was dissolved in 10 mL of ethanol and combined with the above suspension, and stirred for a further 20 minutes. The resulting mixture was then transferred to a Teflon-lined autoclave and heated at 200 °C for 10 hours. After the reaction, the mixture was centrifuged and washed three times with deionized water followed by ethanol. Finally, the product was dried under vacuum at 50 °C to obtain Ce-WO_3 (Ce_1-WO_3 and Ce_3-WO_3). The WO_3 was synthesized using the same procedure, but without the addition of $CeCl_3$.

Electrochemical Measurements

The Nafion membrane was pretreated by boiling in H_2O_2 solution (3 wt%), 0.5 M H_2SO_4, and ultrapure water at 80 °C for 1 h, respectively. Electrochemical measurements were carried out in a typical H-type electrolytic cell separated by Nafion 117 membrane. The prepared Ce-WO_3 /CP electrode, platinum gauze electrode and Ag/AgCl electrode were used as the working electrode, counter electrode and reference electrode, respectively. The potentials reported in this work were converted to RHE scale via calibration with the following equation: E (vs RHE) = E (vs Ag/AgCl) + 0.197 + 0.0591 × pH. Before the electrochemical N_2 reduction measurements, N_2 was continuously pumped into the 0.1 M Li_2SO_4 electrolyte for 30 min. Electrochemical N_2 reduction was performed in N_2-saturated 0.1 M Li_2SO_4 electrolyte. The LSV curves were conducted at the scan rate of 10 mV s^{-1} under Ar- or N_2-saturated 0.1 M Li_2SO_4 solution using the CHI 760e electrochemical workstation.

Preparation of WO_3 and Ce-WO_3 electrode

Ce-WO_3/CP (Ce_1-WO_3/CP and Ce_3-WO_3/CP) electrodes were prepared as follows: First, 5 mg of Ce-WO_3 (Ce_1-WO_3 and Ce_3-WO_3) catalyst and 20 μL of Nafion solution (5 wt%) were dispersed in 980 μL of a mixed solution containing ethanol and H_2O (V:V=2:1) by sonication for 30 minutes to form a homogeneous ink. Then, 20 μL of the Ce-WO_3 ink was loaded onto a carbon paper (1 cm × 1 cm) and dried. WO_3/CP were prepared using the same method.

Determination of NH_3

Concentration of produced NH_3 was determined by the indophenol blue method. In detail, 2 mL post-tested solution was removed from the cathodic chamber, and then added into 2 mL 1.0 M NaOH solution containing $C_7H_6O_3$ and $C_6H_5Na_3O_7 \cdot 2H_2O$ (5 wt%). Next, 1 mL NaClO (0.05 M) and 0.2 mL $Na_2[Fe(NO)(CN)_5] \cdot 2H_2O$ (1 wt%) aqueous solutions were added sequentially. The mixture was allowed to stand at room temperature for 2 hours, after which the UV-Vis absorption spectrum was measured. Calibration of the concentration-absorbance curve was performed using standard NH_4Cl solutions with concentrations ranging from 0.1 to 1.2 μg mL^{-1}, which were prepared by diluting a 100 μg mL^{-1} NH_4Cl solution with 0.1 M Li_2SO_4. The concentration of indophenol blue was determined by measuring the absorbance at a wavelength of 655 nm. A linear relationship between absorbance value and NH_4Cl concentration was observed with a fitting curve of $y = 0.30284x + 0.0337$ ($R^2 = 0.999$), which was obtained from three independent calibrations.

^{15}N isotope labeling experiment

$^{15}N_2$ with a ^{15}N enrichment of 99% (from Aladdin) was used to carry out the isotopic labeling experiment in a 0.1 M Li_2SO_4 electrolyte. The reactor was encapsulated, degassed, and injected with Ar for several times, and finally filled with $^{15}N_2$. After electrolysis at -0.5 V vs RHE for 2 h with the injection of 20 mL $^{15}N_2$ every 10 min, 30 mL of the electrolyte was taken out and concentrated to 1 mL by heating at 75 °C. Then, 0.1 mL of the resultant solution was thoroughly mixed with 0.6 mL of the dimethyl sulphoxide-D6 (99.9% D, from Adamas) for the ^1H nuclear magnetic resonance (NMR) measurement on a Bruker Avance III HD 500 NMR spectrometer. For comparison, $^{14}N_2$ experiment was also operated in the same method.

Determination of N_2H_4

The hydrazine present in the electrolyte was estimated via the method of Watt and Chrisp. A mixture of p-$C_9H_{11}NO$ (5.99 g), HCl (concentrated, 30 mL) and C_2H_5OH (300 mL) was used as a color reagent. In detail, 2 mL electrolyte was removed from the electrochemical reaction vessel and added into 2 mL above prepared color reagent and stirring 20 min at room temperature. The absorbance of the resulting solution was measured at 455 nm. The concentration absorbance curves were calibrated using standard $N_2H_4 \cdot H_2O$ solution with a series of concentrations. The fitting curve ($y = 1.3741x + 0.0007$, $R^2 = 0.9999$) shows a good linear relation of absorbance value with N_2H_4 concentration.

Calculations of NH_3 formation rate and Faradaic efficiency (FE)

The NH_3 yield rate was calculated using the following equation:

$$V\left(\mu g\ h^{-1} mg_{cat}^{-1}\right) = \frac{C_{NH_3} \times V}{t \times m_{cat}}$$

The FE was calculated according to the following equation:

$$FE = \frac{3 \times F \times C_{NH_3} \times V}{17 \times Q}$$

where C_{NH_3} (μg mL^{-1}) is the measured concentration of NH_3; V (mL) is the volume of electrolyte (30 mL); t (s) is the reduction reaction time; m_{cat} (mg) is the mass loading of catalyst on CP; F is Faraday constant (96500 C mol^{-1}); Q (C) is the quantity of applied charge/electricity.

In-situ Raman spectroscopy measurements

In-situ Raman spectroscopy measurements were conducted on the Witec Alpha 300R Raman system, and data was collected at 5 seconds of exposure time averaged over 20 scans. Potentiation tests were performed at -0.5 V vs. RHE in a customized Teflon cell with a quartz window, and the electrolyte was flowed by the peristaltic pump. The self-supported material as the working electrode was immersed in the electrolyte, and the electrode plane was kept perpendicular to the laser. The Raman spectroscopy was recorded.

In-situ ATR-FTIR measurements

In-situ ATR-FTIR was performed on the Thermo Scientific Nicolet iS50 spectrometer equipped with a liquid N_2-cooled MCT-A detector. The self-supported material as the working electrode was press against the silicon crystal covered by a gold film, forming a thin electrolyte layer between the working electrode and the silicon crystal. Potentiation tests were performed at -0.5 V vs. RHE in a customized Teflon cell, and the electrolyte was flowed by the peristaltic pump. Background spectrum was taken at the open circuit potential. FTIR spectra were recorded.

In situ XAS experiments

The in situ XAFS measurements of the W L_3-edge spectra were carried out at 1W1B station in Rapid XAFS. A customized Spectro Electrochemical Cell for in situ XAFS experiments was used, which consisted of a transparent PMMA flat wall and a circular hole (1.5 cm in diameter). The prepared CP with Ce-WO_3 (2×2 cm^2) were wrapped with the waterproof tape to cover the X-ray beam. In the cell, an Ag/AgCl reference electrode and a platinum foil as counter electrode were used. Ce-WO_3 with conductive copper foil as the working electrode and 0.1 M Li_2SO_4 solution was used as electrolyte. The data reduction, analysis and EXAFS fitting were performed using the Athena and Artemis programs from the Demeter data analysis package. The FEFF6 program was used for EXAFS data fitting. Energy calibration was performed utilizing a standard W foil, which was measured as a reference. A linear function was subtracted from the pre-edge region, followed by normalization of the edge jump using Athena software. The k^2-weighted $\chi(k)$ data were Fourier transformed after the application of a Hanning window function ($\Delta k=1.0$). For EXAFS modeling, global amplitude parameters (CN, R, σ^2, and ΔE_0) were derived through nonlinear least-squares refinement of the EXAFS equation applied to the Fourier-transformed data in R-space, utilizing Artemis software. The wavelet transform data were generated by inputting relevant parameters into the HAMA software.

Computational Details

Spin-polarized density functional theory (DFT) simulations were performed to calculate the adsorption of N_2 molecule using the Vienna ab initio simulation package (VASP). The Perdew-Burke-Ernzerhof (PBE) functional within the framework of generalized gradient approximation (GGA) was applied to describe the exchange-correlation interactions. DFT-D2 method was adopted to consider the van der Waals (vdW) interaction. For structural optimization, the Brillouin zone was sampled by 4×3×1 k-points for plane-wave basis, together with an energy cutoff of 500 eV. The WO_3 (010) facet has been cleaved with a vacuum layer of 20 Å to build the WO_3 and Ce-WO_3 slab models. All the atoms were allowed to relax until the residue forces on each atom were less than 0.02 eV/Å. The convergence criterions were set to 10^{-5} eV for total energy. Specially, the value of U in Ce 4f and W 5d is 6 and 6.2, respectively, which is applied to each calculation. In order to avoid interactions between periodic images, a vacuum space of 20 Å was applied to all calculations. The formation Gibbs free energy (ΔG) of the NRR intermediates is calculated as:

$$\Delta G = \Delta E + \Delta ZPE - T\Delta S$$

where ΔE is the electronic energy difference directly obtained from DFT calculations, ΔZPE is the change of zero-point energies, T is the temperature (T=298.15 K), and ΔS is the entropy changes. The entropy of gas molecules is taken from standard values.

MATLAB Simulation Methods

Simulation study of electric field was conducted using MATLAB.

The intensity of electric field can be expressed as

$$Up = \sum_{i=1}^{n} \frac{kQ_i}{r_i}$$

$k = 9\times10^{9}$ N m^2 /C^2 (electrostatic force constant)

$e = -1.6\times10^{-19}$C(electriccharge)

$Å = 10\times10^{-10}$ m

Where U_p, Q_i and r_i are the intensity of the electric field, the charge on atoms, and the relative location of atoms, respectively.

Results and Discussion

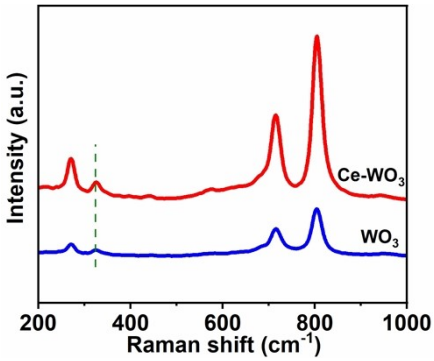

Fig. S1 Raman spectra of WO_3 and Ce-WO_3.

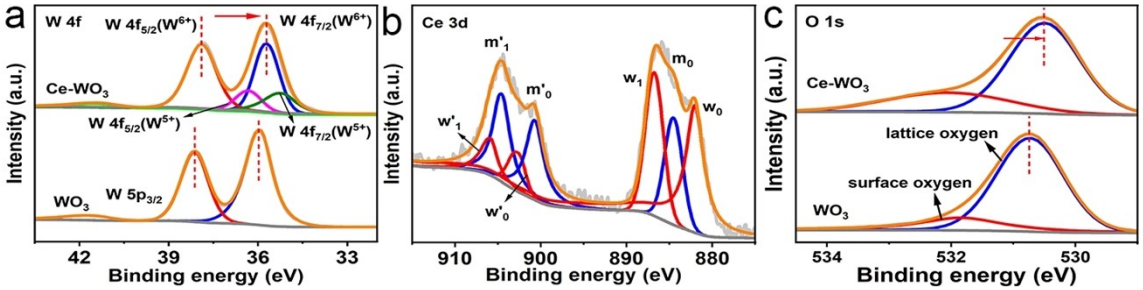

Fig. S2 (a) W 4f XPS spectra of WO_3 and Ce-WO_3. (b) XPS spectra of Ce 3d for Ce-WO_3. (c) XPS spectra of O 1s for WO_3 and Ce-WO_3.

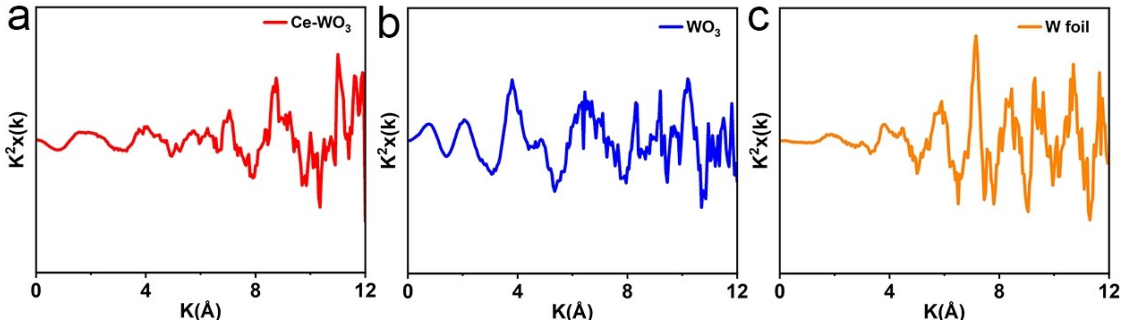

Fig. S3 W L_3-edge EXAFS oscillation spectra of (a) Ce-WO_3, (b) WO_3 and (c) W foil.

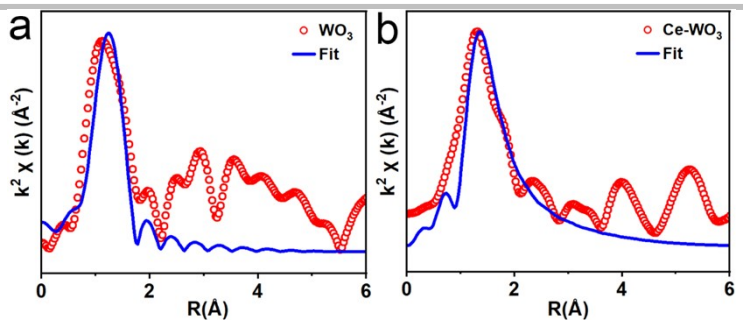

Fig. S4 (a-b) EXAFS of R-space fitting curve of W for WO_3 and Ce-WO_3.

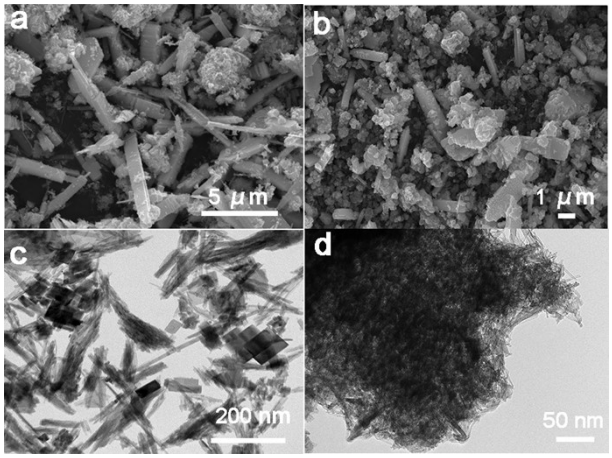

Fig. S5 (a) SEM images of WO_3. (b) SEM images of Ce-WO_3. (c) TEM images of WO_3. (d) TEM images of Ce-WO_3.

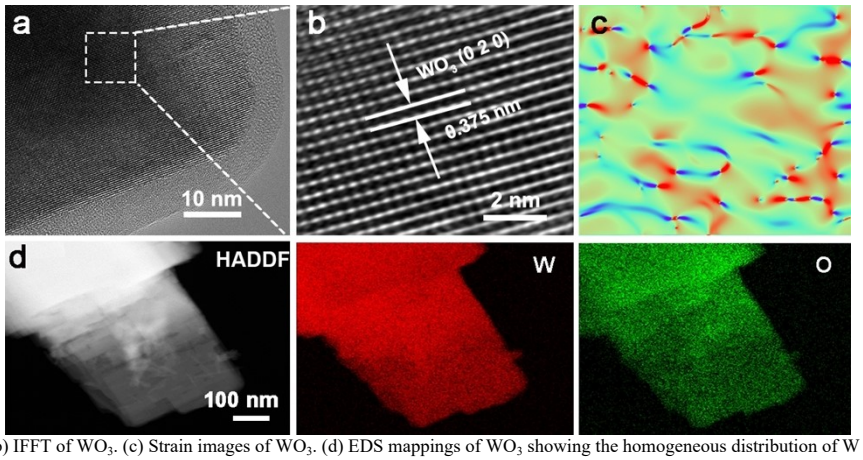

Fig. S6 (a) HR-TEM of WO_3. (b) IFFT of WO_3. (c) Strain images of WO_3. (d) EDS mappings of WO_3 showing the homogeneous distribution of W (red) and O (green).

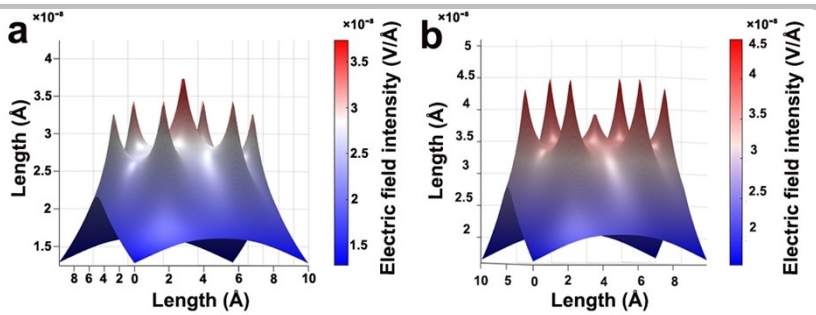

Fig. S7 (a-b) MATLAB simulation of local electric field on WO_3 and Ce-WO_3.

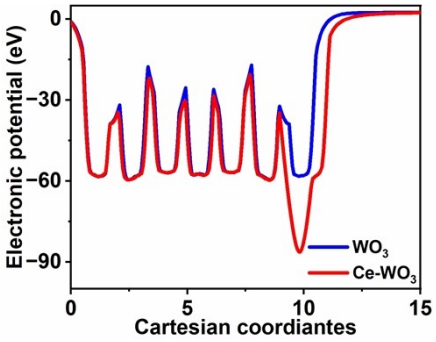

Fig. S8 ESP curves of WO_3 and Ce-WO_3.

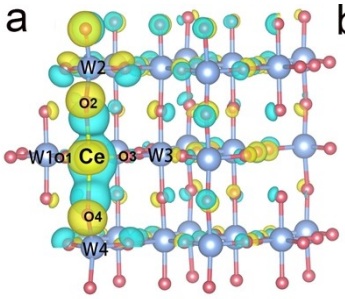

b

Atom	Bader charge (e)
Ce	-2.12
O1	+0.16
O2	+0.02
O3	+0.17
O4	+0.04
W1	+0.02
W2	+0.25
W3	+0.03
W4	+0.23

Fig. S9 (a) Charge density difference of Ce-WO_3. (b) Bader charge in Ce-O-W unit sites.

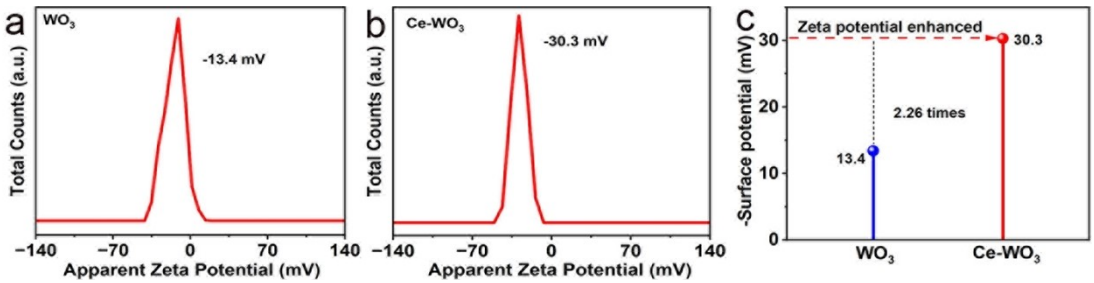

Fig. S10 Zeta potential of (a) WO_3 and (b) Ce-WO_3. (c) The Zeta potential of WO_3 and Ce-WO_3 samples.

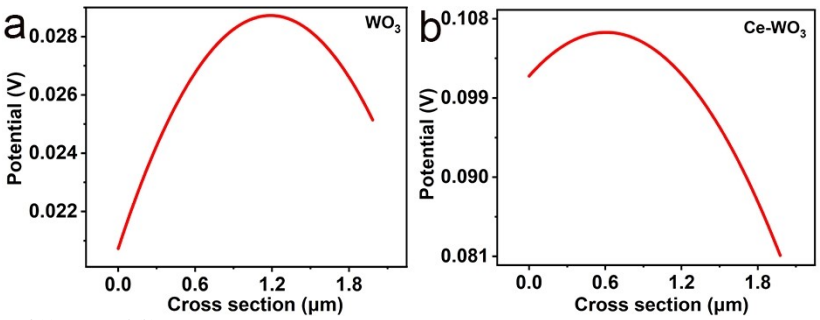

Fig. S11 The potential distributions of (a) WO_3 and (b) Ce-WO_3.

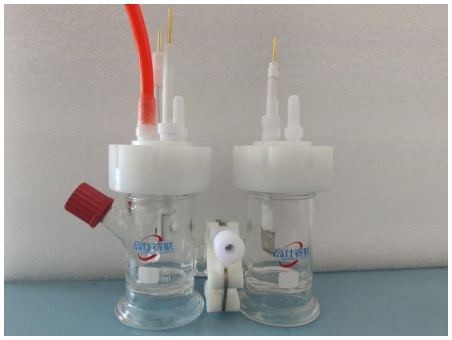

Fig. S12 The home-made reactor for ENRR.

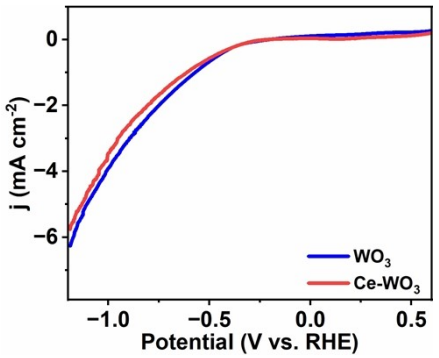

Fig. S13 LSV curves of WO_3 and Ce-WO_3 for the HER.

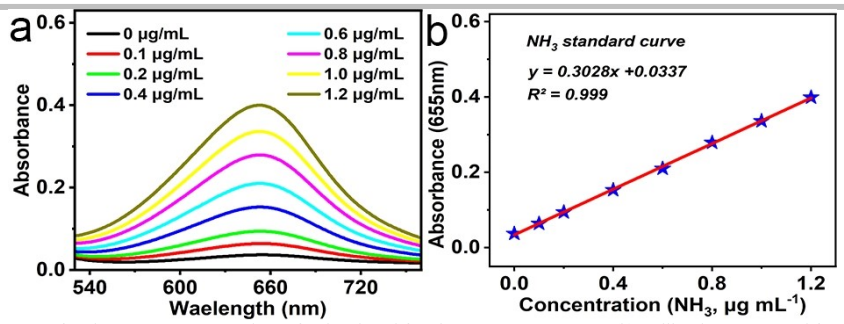

Fig. S14 (a) UV-vis absorption spectra of various NH_4^+ concentrations after incubated for 2h at room temperature. (b) Calibration curve used for calculating NH_4^+ concentrations.

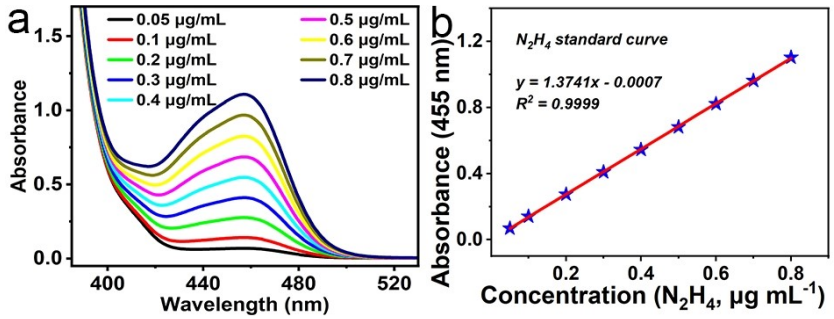

Fig. S15 (a) UV-vis absorption spectra of various N_2H_4 concentrations after incubated for 20 min at room temperature. (b) Calibration curve used for calculating N_2H_4 concentrations.

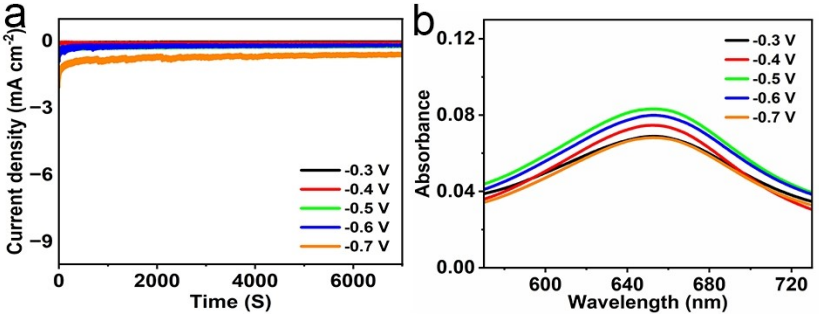

Fig. S16 (a) Chronoamperometry curves of WO_3 at different potentials in N_2-saturated 0.1 M Li_2SO_4. (b) UV-Vis absorption spectra of WO_3.

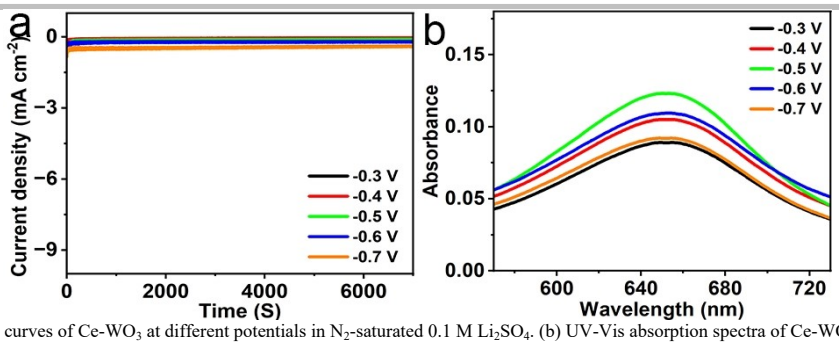

Fig. S17 (a) Chronoamperometry curves of Ce-WO_3 at different potentials in N_2-saturated 0.1 M Li_2SO_4. (b) UV-Vis absorption spectra of Ce-WO_3.

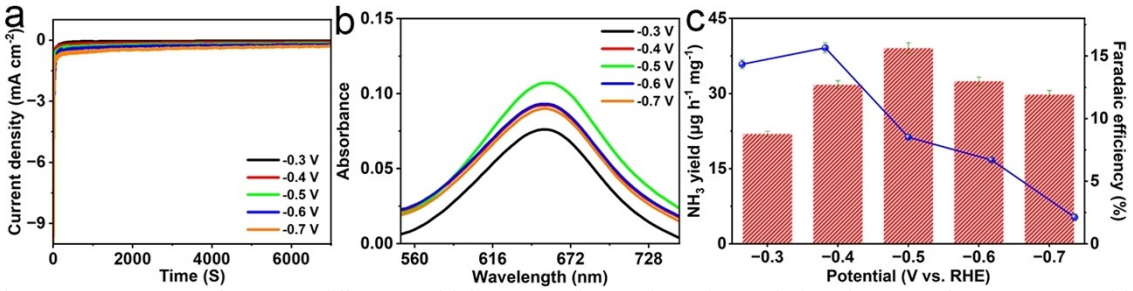

Fig. S18 (a) Chronoamperometry curves of Ce_1-WO_3 at different potentials in N_2-saturated 0.1 M Li_2SO_4. (b) UV-Vis absorption spectra of Ce_1-WO_3. (c) NH_3 yields and FEs of Ce_1-WO_3.

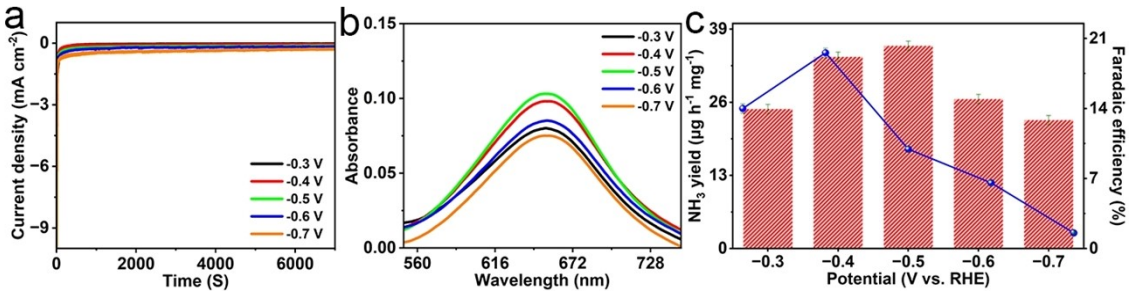

Fig. S19 (a) Chronoamperometry curves of Ce_3-WO_3 at different potentials in N_2-saturated 0.1 M Li_2SO_4. (b) UV-Vis absorption spectra of Ce_3-WO_3. (c) NH_3 yields and FEs of Ce_3-WO_3.

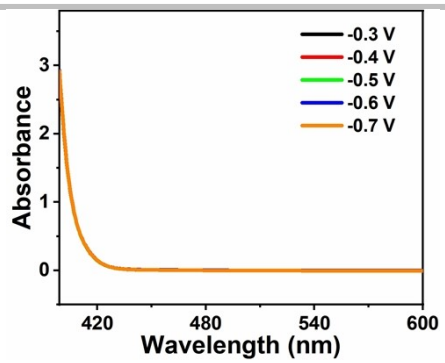

Fig. S20 UV-vis absorption spectra of the hydrazine.

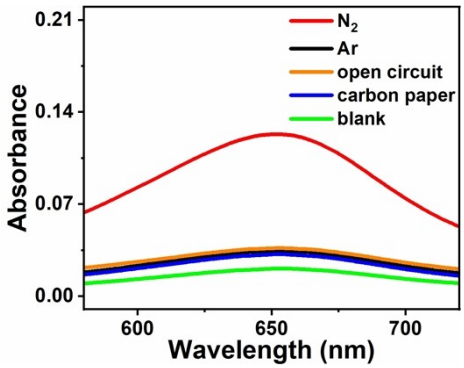

Fig. S21 UV-vis absorption spectra under different control experiments.

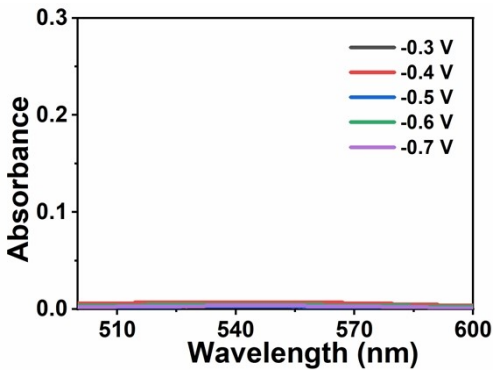

Fig. S22 The UV-vis absorbance spectra of NO_2^-.

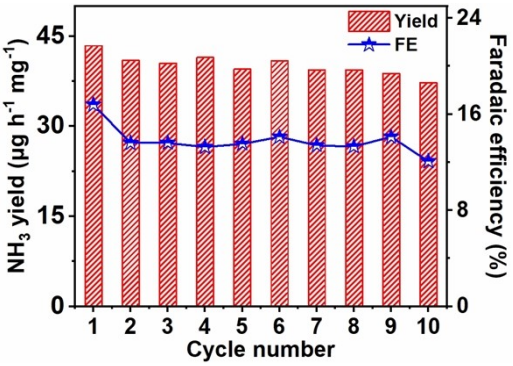

Fig. S23 Cycling test for Ce-WO_3 at -0.5 V vs RHE.

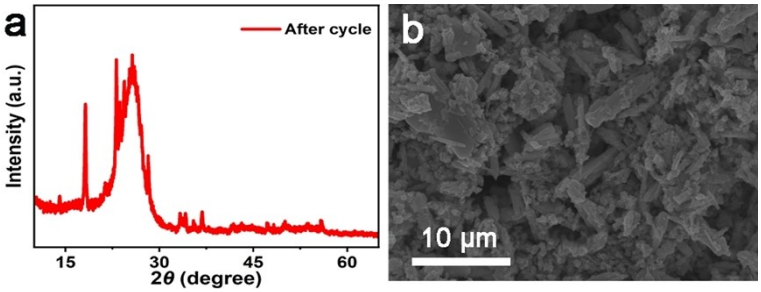

Fig. S24 (a) XRD and (b) SEM image of Ce-WO_3 after stability test.

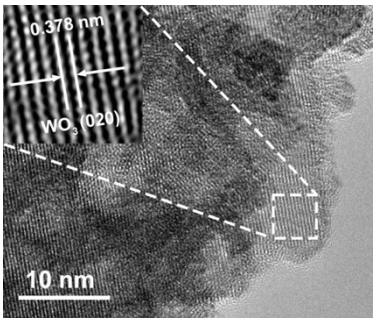

Fig. S25 TEM image of Ce-WO_3 after stability test.

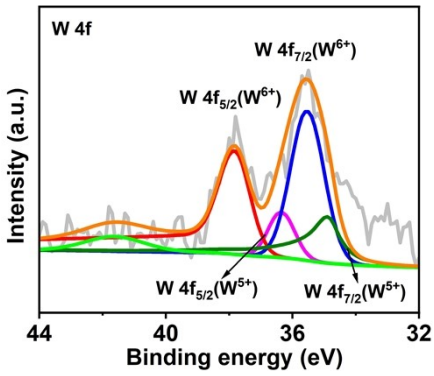

Fig. S26 W 4f XPS spectra e of Ce-WO_3 after stability test.

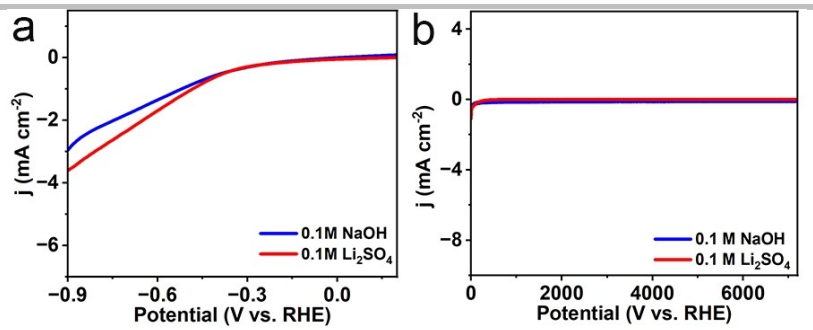

Fig. S27 (a) LSV curves of Ce-WO_3 and (b) chronoamperometry curves of Ce-WO_3 in the 0.1 M Li_2SO_4 and 0.1 M NaOH at -0.5 V vs RHE.

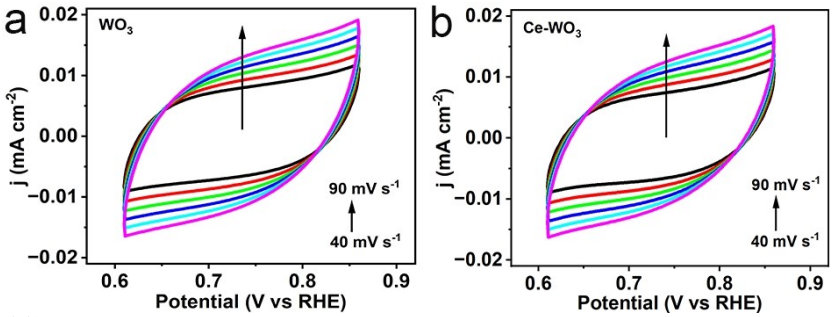

Fig. S28 CV curves of (a) WO_3 and (b) Ce-WO_3.

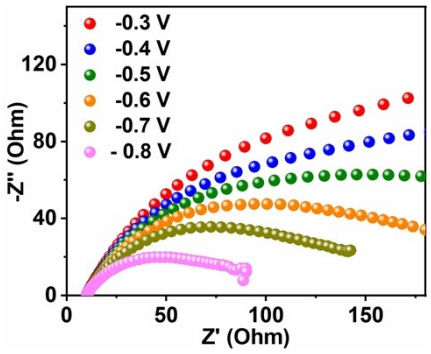

Fig. S29 Nyquist plots of WO_3.

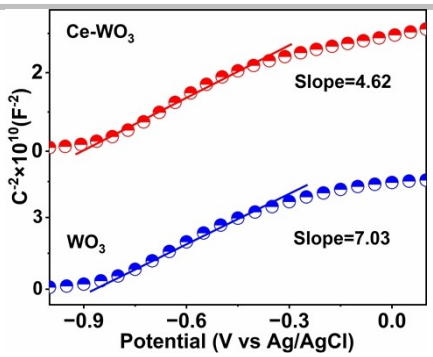

Fig. S30 Mott-Schottky plots of WO_3 and Ce-WO_3.

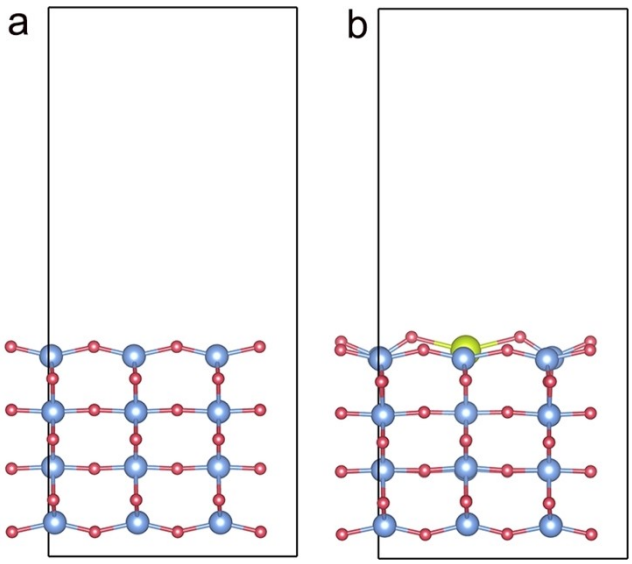

Fig. S31 The side view of optimized structure for (a) WO_3 and (b) Ce-WO_3.

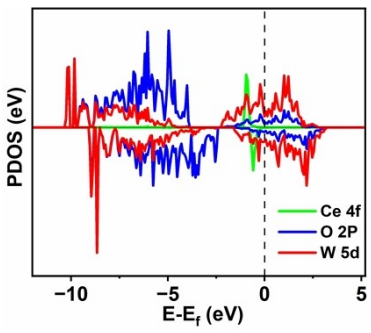

Fig. S32 PDOS of Ce-WO_3.

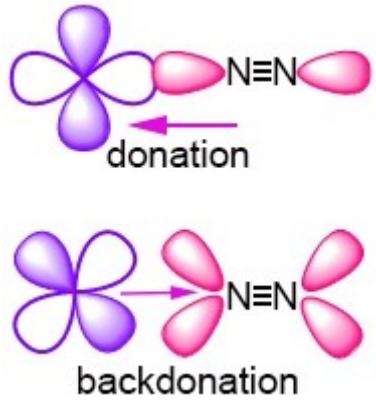

Fig. S33 Schematic of electron feedback mechanism from d orbitals of W to π* of N_2.

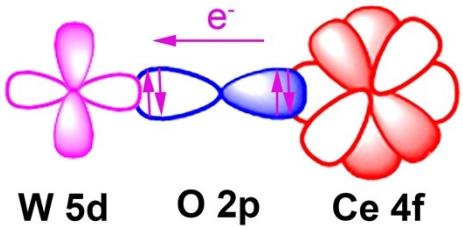

Fig. S34 The schematic diagram displaying Ce bonding to O and transition metal W species

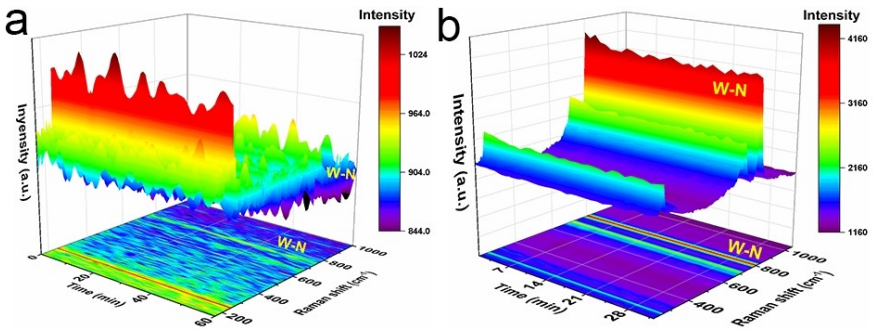

Fig. S35 In situ Raman spectra of (a) WO_3 and (b) Ce-WO_3.

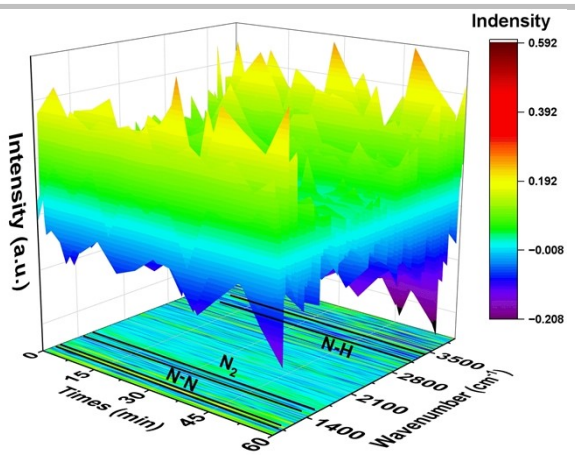

Fig. S36 In situ FTIR spectra of Ce-WO_3.

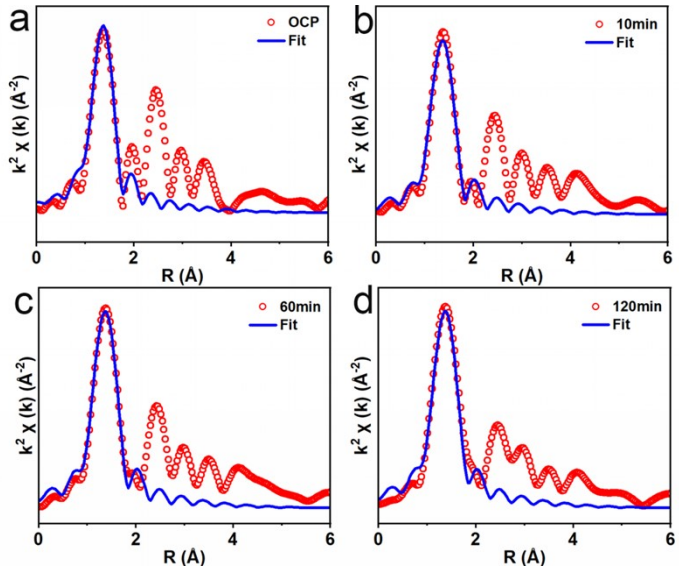

Fig. S37 EXAFS fitting spectrum for Ce-WO_3.

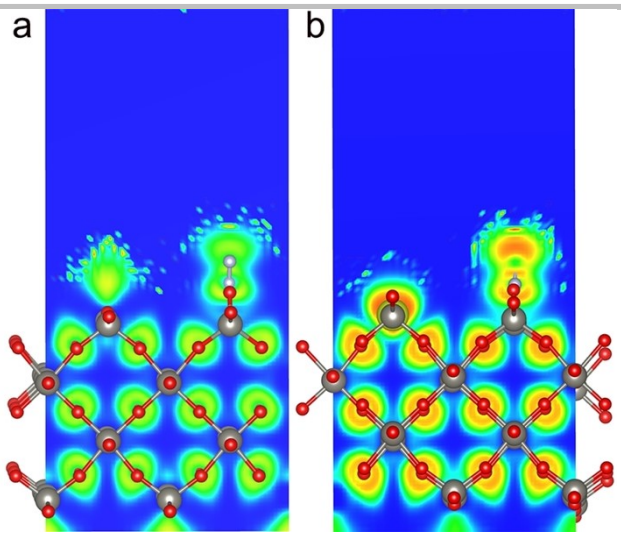

Fig. S38 The ELF of N_2 on the (a) WO_3 and (b) Ce-WO_3.

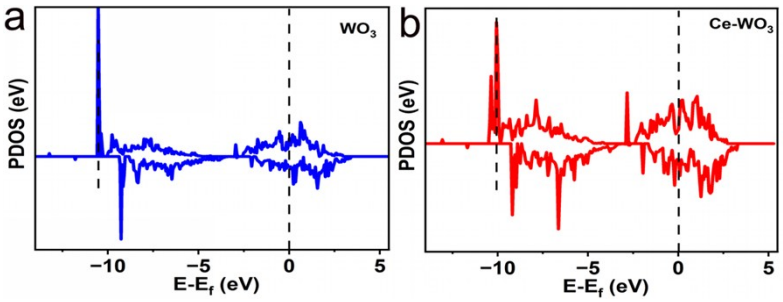

Fig. S39 DOS of the N_2 on the (a) WO_3 and (b) Ce-WO_3.

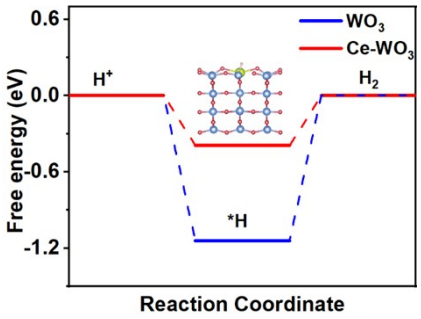

Fig. S40 Free-energy diagrams of HER on the WO_3 and Ce-WO_3.

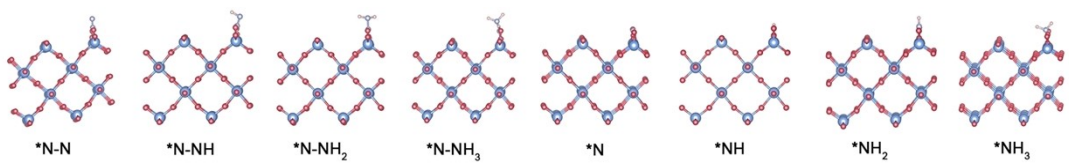

Fig. S41 The optimized structures of different intermediates for WO_3 during NRR.

Table S1. Curve fit Parameters[a] for W K-edge EXAFS for WO_3 and Ce-WO_3 standard.

sample	Scattering pair	CN	R(Å)	s^2/Å^2	ΔE_0(ev)	R factor
Ce-WO_3	W-O	2.2±0.3	1.90±0.02	0.001±0.004	1.0±0.5	0.028
WO_3	W-O	3.0±0.3	1.72±0.03	0.003±0.005	1.0±0.5	0.028

S02 is the amplitude reduction factor; CN is the coordination number; R is interatomic distance (the bond length between central atoms and surrounding coordination atoms); σ2 is Debye-Waller factor (a measure of thermal and static disorder in absorber-scatterer distances); ΔE0 is edge-energy shift (the difference between the zero kinetic energy value of the sample and that of the theoretical model). R factor is used to value the goodness of the fitting.

Ce-WO_3: (FT range: 3.0-10.0 Å-1; fitting range: 1-2 Å)

WO_3: (FT range: 3.0-10.0 Å-1; fitting range: 1-2 Å)

Table S2. ICP-MS results of the Ce-WO_3 and WO_3 samples.

Catalysts	Content of Ce (wt.%)
Ce-WO_3	2.9634
WO_3	0

Table S3 Structural parameters extracted from the W L_3-edge EXAFS fitting.

sample (Ce-WO_3)	Scattering pair	CN	R(Å)	σ^2/Å	ΔE_0(ev)	R factor
OCP	W-O	2.41±0.01	1.785±0.01	0.001±0.001	1.0±0.5	0.018
10min	W-O	2.42±0.01	1.792±0.01	0.001±0.001	1.0±0.5	0.018
60min	W-O	2.62±0.01	1.797±0.01	0.002±0.001	1.0±0.5	0.018
120min	W-O	2.90±0.01	1.802±0.01	0.003±0.001	1.0±0.5	0.018

(S02=1)

S02 is the amplitude reduction factor; CN is the coordination number; R is interatomic distance (the bond length between central atoms and surrounding coordination atoms); σ2 is Debye-Waller factor (a measure of thermal and static disorder in absorber-scatterer distances); ΔE0 is edge-energy shift (the difference between the zero kinetic energy value of the sample and that of the theoretical model). R factor is used to value the goodness of the fitting.

Ce-WO_3: (FT range: 3.0-10.0 Å^{-1}; fitting range: 1-2 Å)

Table S4. Comparison of electrocatalytic N_2 reduction performance with other reported electrocatalysts recently.

Catalysts	Electrolyte	Yield (NH_3)	FE (NH_3)	Ref.
Ce-WO_3	0.1 M Li_2SO_4	47.11 μg h^{-1} mg_{cat}^{-1}	25.49%	This work
$Co_{0.05}W_{0.95}C$	0.1 M H_2SO_4	32.49 μg h^{-1} mg_{cat}^{-1}	27.17%	[1]
WO_3-C_3N_4	0.1 M Li_2SO_4	54.87 μg h^{-1} mg_{cat}^{-1}	24.33 %	[2]
NV-W_2N_3	0.1 M KOH	11.66 μg h^{-1} mg_{cat}^{-1}	11.67%	[3]
$W_{18}O_{49}$	0.25M $LiClO_4$	24.7 μg h^{-1} mg_{cat}^{-1}	20%	[4]
WO_3-C_3N_4-R	0.1 M Li_2SO_4	43.5 μg h^{-1} mg_{cat}^{-1}	11.2%	[5]
W-NO/NC	0.5 M $LiClO_4$	12.62 μg $h^{-1}mg_{cat}^{-1}$	8.35%	[6]
$FeWS_x$@$FeWO_4$	0.1 M KOH	30.2 μg h^{-1} mg_{cat}^{-1}	16.4%	[7]
WS_2-WO_3	0.1 M Li_2SO_4	62.38 μg h^{-1} mg_{cat}^{-1}	24.24%	[8]
WS_2@MoS_2	0.1 M KOH	61.79 μg h^{-1} mg_{cat}^{-1}	21.64%	[9]
PdCu	0.1 M HCl	20.24 μg h^{-1} mg_{cat}^{-1}	13.16%	[10]

References

1. Y. Gao, M.-J. Zhu, X.-H. Liu, G.-L. Dai, Y.-W. Zhou, Z.-D. Meng, L. Luo, T. Gan, F. Chen, Y.-Y. Zhou, W.-W. Deng and S.-Q. Liu, *Chem. Eng. J*, 2024, **493**,152659.
2. X. Wang, J. Li, Y. Ji, S. Li, S. Wang, Y. Sun, X. Gao, Z. Tang, H. Zhang, F. Zhang, J. Xie, Z. Yang and Y.-M. Yan, *Appl. Catal. B Environ*, 2024, **345**,123700.
3. H. Jin, L. Li, X. Liu, C. Tang, W. Xu, S. Chen, L. Song, Y. Zheng and S. Z. Qiao, *Adv. Mater*, 2019, **31**,1902709.
4. Y. Tong, H. Guo, D. Liu, X. Yan, P. Su, J. Liang, S. Zhou, J. Liu, G. Q. Lu and S. X. Dou, *Angew. Chem. Int. Ed*, 2020, **59**,7356-7361.
5. X. Wang, J. Xie, S. Li, Z. Yuan, Y. Sun, X. Gao, Z. Tang, H. Zhang, J. Li, S. Wang, Z. Yang and Y.-M. Yan, *Appl. Catal. B Environ*, 2023, **339**,123126.
6. Y. Gu, B. Xi, W. Tian, H. Zhang, Q. Fu and S. Xiong, *Adv. Mater*, 2021, **33**,2100429.
7. Y. Zhao, F. Li, W. Li, Y. Li, C. Liu, Z. Zhao, Y. Shan, Y. Ji and L. Sun, *Angew. Chem. Int. Ed*, 2021, **60**,20331-20341.
8. X. Wang, S. Li, Z. Yuan, Y. Sun, Z. Tang, X. Gao, H. Zhang, J. Li, S. Wang, D. Yang, J. Xie, Z. Yang and Y. M. Yan, *Angew. Chem. Int. Ed*, 2023, **62**,e202303794
9. B. Cui, M. Cao, J. Weng, Y. Li, C. Wang, J. Liu, Y. Wen, L. Tao and S. Liu, *ACS Appl. Mater. Interfaces*, 2025, **17**,38648-38657.
10. L. Wen, K. Sun, X. Liu, W. Yang, L. Li and H. L. Jiang, *Adv. Mater*, 2023, **60**, 2210669.